



# CHALMERS

## Chalmers Publication Library

### Parameter Estimation and Uncertainty Quantification of a Subframe with Mass Loaded Bushings

This document has been downloaded from Chalmers Publication Library (CPL). It is the author's version of a work that was accepted for publication in:

**Model Validation and Uncertainty Quantification, Volume 3, Proceedings of the 35th IMAC, A Conference and Exposition on Structural Dynamics 2017 (ISSN: 2191-5644)**

Citation for the published paper:

Gibanica, M. ; Abrahamsson, T. (2017) "Parameter Estimation and Uncertainty Quantification of a Subframe with Mass Loaded Bushings". Model Validation and Uncertainty Quantification, Volume 3, Proceedings of the 35th IMAC, A Conference and Exposition on Structural Dynamics 2017, vol. 3 pp. 61-76.

[http://dx.doi.org/10.1007/978-3-319-54858-6\\_7](http://dx.doi.org/10.1007/978-3-319-54858-6_7)

Downloaded from: <http://publications.lib.chalmers.se/publication/249884>

Notice: Changes introduced as a result of publishing processes such as copy-editing and formatting may not be reflected in this document. For a definitive version of this work, please refer to the published source. Please note that access to the published version might require a subscription.

Chalmers Publication Library (CPL) offers the possibility of retrieving research publications produced at Chalmers University of Technology. It covers all types of publications: articles, dissertations, licentiate theses, masters theses, conference papers, reports etc. Since 2006 it is the official tool for Chalmers official publication statistics. To ensure that Chalmers research results are disseminated as widely as possible, an Open Access Policy has been adopted. The CPL service is administrated and maintained by Chalmers Library.

# Parameter estimation and uncertainty quantification of a subframe with mass loaded bushings

Mladen Gibanica<sup>1,2</sup>, Thomas J. S. Abrahamsson<sup>1</sup>

<sup>1</sup>Applied Mechanics, Chalmers University of Technology, Hörsalsvägen 7A, SE-41296 Göteborg, Sweden

<sup>2</sup>Volvo Car Corporation, SE-40531 Göteborg, Sweden

e-mail: [mladen.gibanica@chalmers.se](mailto:mladen.gibanica@chalmers.se)

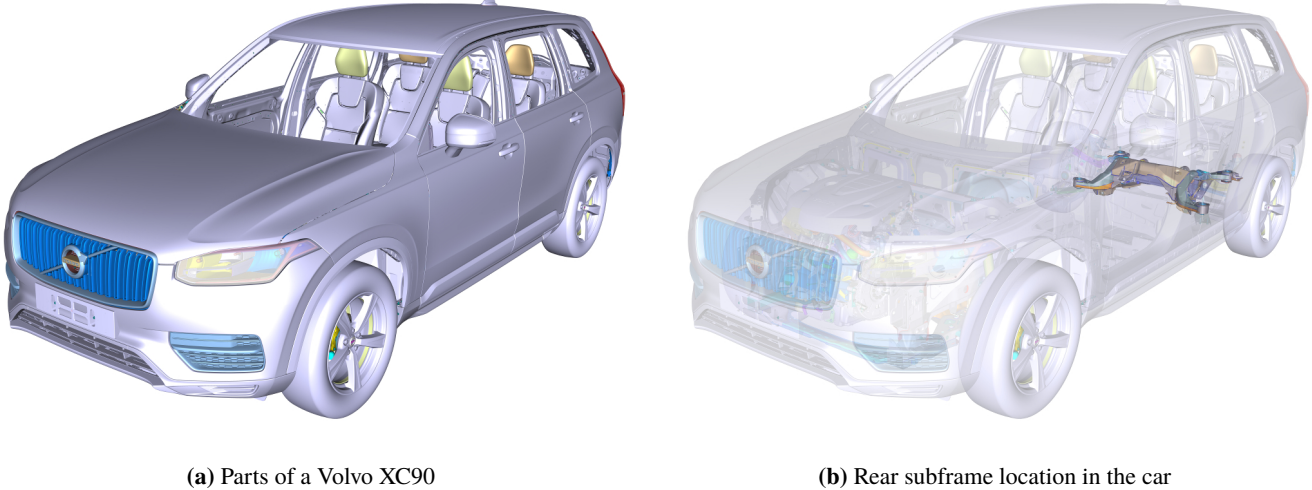
## ABSTRACT

In the automotive industry components are often connected through rubber bushings. The bushings' material properties are usually not well known. In computational models these properties are parametrised and their spread can be considerable. A good estimate of these parameters is important in various applications, including substructuring, and for uncertainty quantification of systems with connected components. This paper deals with the calibration of an industrial size finite element model of a car subframe with parametrised bushing models. Mass loading is used on the bushings to bring local bushing modes to a lower frequency region and impose a more realistic boundary condition in component testing. The model parameters can be calibrated in different ways. In this paper two approaches are considered. They are based on two test configurations, one with and one without mass loaded boundaries. In the first case only the bushing parameters are considered for the mass loaded boundary configuration. In the second case, consisting of two steps, the configuration without mass loaded boundaries is considered in which the bushing parameters are first fixed and other model parameters considered, and in the last step a subset of all parameters is considered. The calibration, validation and uncertainty quantification, using bootstrapping, have been performed using the open-source MATLAB tool FEMcali.

Keywords: Uncertainty quantification, model updating, industrial application, parametrised bushings, FEMcali.

## 1 Introduction

In the automotive industry finalised products are commonly made up of thousands of components, which can in turn be made out of smaller components. These structures are increasingly studied with computer aided engineering (CAE) software, such as finite element (FE) software, due to the flexibility computer models bring in terms of modifying and analysing the structures. There exist many ways of analysing the structures. An approach that is often taken is to divide the structure into substructures and analyse every substructure separately, known as substructuring [1, 2]. The substructures results are assembled and the complete structure's responses can be solved for. For an accurate modelling it is important to understand the physics of every substructure, and especially the physical behaviour at the interfaces through which the substructures are assembled. Many different connection types exist, for different purposes, where bushings are commonly used when it is of interest to control, or suppress the vibration levels from one component to another [3]. Hence, they are commonly used in the automotive industry to connect, for example, subframes to the body in white (BIW). The bushings are partly constructed from rubber materials, and it is well known that the Young's modulus of rubber materials is temperature and frequency dependent and can exhibit large variations between samples [3]. Therefore, synthesised structures through rubber bushings can show a large variation, stemming from the uncertain rubber material properties in the bushings, but also poor prediction capabilities due to unknown, and not modelled, physics. Furthermore, for connected structures, through rubberised bushings, a good damping estimation can be important in the assembly's predictive capabilities. The damping is usually not modelled based on first principles due to its complexity, but rather by calibration of models to experimentally acquired data. Therefore, there is an interest in updating FE models towards experimentally obtained data from vibration tests [4], so that the FE model responses corresponds better to the



(a) Parts of a Volvo XC90

(b) Rear subframe location in the car

**Fig. 1** The rear subframe connects the suspension link arms and the car body, and is thus an important part from a vibration perspective

specific component of interest, but also to obtain the damping characteristics of the structure. In previous studies at Volvo Car Corporation three Volvo V40 subframes [5, 6] and three Volvo XC90 (2015) front subframes [7] have been calibrated towards experimental data. This paper, forming a second study on the Volvo XC90, is concerned primarily with the estimation of the bushing rubber material parameters in a mass loaded boundary configuration of a Volvo XC90 rear subframe, shown in Fig. 1, but also to update the rear subframe model in general. The rear subframe, like the front subframe is important from a vibration perspective as it connects the suspension link arms to the car body. In this paper model updating [8] is proposed as a tool for estimating the bushing model parameters by mass loading the bushings in an experimental modal analysis (EMA). By mass loading the bushings they are activated considerably and bring local bushing modes down in frequency where it is possible to study them with modal analysis. This also provides a good estimate of the additional damping provided by the bushings. Furthermore, mass loading provides a more realistic boundary condition on the bushings, i.e. closer to the assembled behaviour which is sought. In Fig. 2 the two different bushing types are shown along with the mass loading component in Fig. 2c and a small region of an FE representation of the mass loaded bushing boundary configuration in Fig. 2d.

In this paper the calibration is performed with the open-source application FEMcali, described in [9–11]. Two finite element models are used, one with and one without mass loaded boundary configuration. The FE models of both configurations consist of over half a million degrees of freedom each. In the calibration procedure a parametrised surrogate model of the FE model is first created. The calibration method then seeks to obtain a calibrated parameter setting such that the deviation between the FE model's frequency response functions (FRFs) and the experimentally identified model's FRFs is minimised. Normalised damping is imposed on both models to circumvent the mode pairing problem. A relatively high damping also yields a smooth deviation metric [9]. The calibrated parameter setting is then used as a starting point in an optimisation procedure using bootstrapping to quantify the parameter uncertainties. Previous studies using the same calibration procedure on various structures have produced mostly good results, see [5–7, 12, 13]. Pretest planning is performed on a coarse FE model using the effective independence (Efi) method [14, 15] with an added gramian rejection step, described further in [16]. In this paper a single input multiple output (SIMO) stepped sine testing procedure is used, with multiple simultaneous sinusoidal inputs for faster test procedure utilising an improved frequency strategy proposed in [17] for subspace state-space system identification [18]. First the FE model with mass loading is calibrated towards experimental data for a good parameter estimation of the rubber's Young's modulus, i.e. all other model parameters are fixed at their nominal values. Then the configuration without mass loading is calibrated, with fixed but updated rubber parameters, for an overall good parameter estimation of the rear subframe FE model. In a final step a subset of all parameters are updated towards a higher frequency region for the configuration without mass loading to gain further physical understanding of the component.

Even though it is known that mass produced components exhibit varying dynamic and static properties, and it has been shown that a spread in the behaviour between front subframe individuals of a Volvo XC90 [7] is noticeable, this paper is concerned with only one rear subframe of said car model due to less observed variability between the rear subframes. This was experimentally verified from experiments on three rear subframes.

Rubber can be characterised as a viscoelastic material [3]. It is known that its Young's modulus is frequency and temperature dependent [3], which is also shown in [19] for some specific rubber materials. In this paper the rubber material is modelled



(a) Bushing 1

(b) Bushing 2

(c) Additional mass

(d) Assembly

**Fig. 2** In (a) one bushing is depicted and in (b) the other bushing. In (c) the additional mass is shown and in (d) the assembly of the additional mass and the rear subframe, for one bushing

with solid elements and an isotropic linear material model, which according to [3] is sufficient as the bushing parameters are estimated from the mass loaded configuration and the frequency region of interest is small enough for the Young's modulus frequency dependency to be disregarded. Small strains are assumed and non-linear effects are not regarded. Temperature effects are also disregarded.

The theory behind the model updating procedure used in this paper is presented briefly in Section 2. In Section 3 the vibration testing procedure, FE models and parameter selection are described. The results are presented in Section 4 and in Section 5 the work is concluded.

## 2 Theory

The theory behind the model updating procedure is briefly introduced here. For a full explanation of the theory behind the deterministic model calibration, see [9], and for the model parameter uncertainty quantification theory see [10, 11].

The goal of the calibration is to estimate a calibration parameter setting  $\mathbf{p}_b$  that minimises the deviation between the experimentally obtained FRFs  $\mathbf{H}_X(\omega_i) \in \mathbb{C}^{n_y \times n_u}$  and the FE model FRFs  $\mathbf{H}_{FE}(\omega_i) \in \mathbb{C}^{n_y \times n_u}$  at  $n_f$  frequency steps  $\omega_i$  where  $n_y$  and  $n_u$  denote the number of outputs and inputs, respectively. It is possible to express  $\mathbf{H}_X(\omega_i)$ , see [10, 11, 20, 21], as

$$\mathbf{H}_X(\omega_i) = \mathbf{H}_R(\omega_i) + \mathbf{N}_o(\omega_i) = (\mathbf{H}_{FE}(\omega_i) + \mathbf{N}_m(\omega_i)) + \mathbf{N}_o(\omega_i) = \mathbf{H}_{FE}(\omega_i) + \mathbf{N}_G(\omega_i), \quad i = 1, \dots, n_f \quad (1)$$

where  $\mathbf{H}_R(\omega_i) \in \mathbb{C}^{n_y \times n_u}$  denote the true frequency response of the real structure,  $\mathbf{N}_G(\omega_i) \in \mathbb{C}^{n_y \times n_u}$  is the observed prediction error which can be represented as  $\mathbf{N}_G(\omega_i) = \mathbf{N}_m(\omega_i) + \mathbf{N}_o(\omega_i)$  where  $\mathbf{N}_m(\omega_i)$  denote the model prediction error and  $\mathbf{N}_o(\omega_i)$  denote the measurement noise. Assuming that the bias introduced by the FE model is small,  $\mathbf{N}_{G_{r,s}}$ , for  $r = 1, \dots, n_y$  and  $s = 1, \dots, n_u$ , can be modelled as an independent, zero mean, circularly complex normally distributed random variable with a known variance  $\sigma^2$ .

The calibration procedure consist of three steps, as explained in [10, 11]. First an EMA is performed in which the used discrete frequencies are selected according to [17] and a system  $\Sigma$  is identified from the experimental data using N4SID, such that its transfer function representation  $\mathbf{H}_\Sigma$  asymptotically fulfils the criterion  $\lim_{n_f \rightarrow \infty} \|\mathbf{H}_R - \mathbf{H}_\Sigma\|_\infty = 0$  as shown in [18]. N4SID is a linear subspace state-space system identification method [18] implemented in MATLAB's System Identification toolbox [22] which enables the evaluation of the experimental system at arbitrary frequencies. The experimental data set  $\mathbf{H}_X$  is split into two data sets after this stage, i.e. poorly identified channels are used as validation data in a validation set denoted  $\mathbf{H}_V$  and the remaining channels in a calibration set denoted  $\mathbf{H}_X$ . The channels used in the validation data set are thus also removed from the identified system  $\Sigma$ . Further details of the system identification is given in Section 3.1.

The second step consists of a deterministic calibration procedure in which a calibration parameter setting  $\mathbf{p}^*$  is estimated from the nominal FE model parameter setting  $\mathbf{p}_0$  towards the identified system  $\mathbf{H}_\Sigma$ , with equalised damping in both models. A deviation metric, that is smooth and weights high and low structural responses equally is used in the Levenberg–Marquardt optimisation algorithm [23–25], and can be formed as

$$\mathbf{p}^* = \arg \min_{\mathbf{p}} \frac{\epsilon^H(\mathbf{p})\epsilon(\mathbf{p})}{N} \quad \text{with} \quad \epsilon(\mathbf{p}) = \log_{10} \text{vect}(\mathbf{H}_{FE}(\mathbf{p})) - \log_{10} \text{vect}(\mathbf{H}_\Sigma) \quad (2)$$

where  $\mathbf{H}_{FE}(\mathbf{p})$  represents the FE model, at parameter setting  $\mathbf{p}$ , and the superscript  $H$  denote the conjugate transpose. Here  $\text{vect}(\cdot)$  stands for the vectorisation operation in which a matrix is transformed into a vector by stacking the columns of the matrix such that the transfer function matrices in Equation (2) are transformed into an  $n_y n_u n_f \times 1$  column vector. The objective function is non-linear and thus many start parameter settings are used, generated by the Latin hypercube sampling technique [26], from

which  $\mathbf{p}^*$  is selected from the best calibration outcome. After the calibration a mode pairing algorithm [27] is used to map the experimental damping to the correct FE model modes. The theoretical framework for this step is explained in Section 2.1.

The last step considers the parameter uncertainty, in which the calibrated parameter configuration  $\mathbf{p}^*$  is used as an initial start location in an undamped Gauss-Newton optimisation procedure [25] to find the parameter configuration  $\mathbf{p}_b$  that minimises the deviation metric, at some parameter setting  $\mathbf{p}$ ,

$$\mathbf{p}_b = \arg \min_{\mathbf{p}} \frac{\gamma^H(\mathbf{p})\gamma(\mathbf{p})}{N} \quad \text{with} \quad \gamma(\mathbf{p}) = \log_{10} \text{vect}(\mathbf{H}_{FE}(\mathbf{p})) - \log_{10} \text{vect}(\mathbf{H}_X^b) \quad (3)$$

where  $\mathbf{H}_X^b$  represent bootstrap samples [28] drawn from  $\mathbf{H}_X$ . This procedure is repeated  $n_b$  times on different data sets and hence the measurement noise influence on the model parameters can be obtained, which is further explained in Section 2.2.

## 2.1 Deterministic model updating procedure

The calibration procedure utilises the mass and stiffness matrices formed from an FE representation of the structure of interest. Such mechanically vibrating systems can be written as [1]

$$\mathbf{M}\ddot{\mathbf{q}} + \mathbf{V}\dot{\mathbf{q}} + \mathbf{K}\mathbf{q} = \mathbf{f}(t) \quad (4)$$

where the dot notation is used for time differentiation and  $\mathbf{M}$ ,  $\mathbf{V}$  and  $\mathbf{K} \in \mathbb{R}^{m \times m}$  represent the mass, damping and stiffness matrices, respectively. The general displacement vector is denoted by  $\mathbf{q}$  and the external force vector by  $\mathbf{f}(t)$ .

Systems on second order form, such as in Equation (4), can be cast into first order form by forming a state vector  $\mathbf{x} = [\mathbf{q}^T, \dot{\mathbf{q}}^T]^T$  which gives

$$\begin{cases} \dot{\mathbf{x}} = \mathbf{Ax} + \mathbf{Bu} \\ \mathbf{y} = \mathbf{Cx} + \mathbf{Du} \end{cases} \quad (5)$$

with  $\mathbf{A} \in \mathbb{R}^{n \times n}$  representing the system matrix,  $\mathbf{B} \in \mathbb{R}^{n \times n_u}$  representing the input matrix,  $\mathbf{C} \in \mathbb{R}^{n_y \times n}$  representing the output matrix,  $\mathbf{D} \in \mathbb{R}^{n_y \times n_u}$  representing the force throughput matrix and  $\mathbf{y}$  representing the system outputs. The load vector  $\mathbf{f}$  in Equation (4) can be formed from the input vector  $\mathbf{u} \in \mathbb{R}^{n_u}$  with the Boolean transformation matrix  $\mathbf{U}$  as  $\mathbf{f} = \mathbf{U}\mathbf{u}$ . The relationship between the state dimension  $n$  and degrees of freedom  $m$  is  $n = 2m$ . The system matrices can then be formed as

$$\mathbf{A} = \begin{bmatrix} \mathbf{0} & \mathbf{I} \\ -\mathbf{M}^{-1}\mathbf{K} & -\mathbf{M}^{-1}\mathbf{V} \end{bmatrix} \quad \mathbf{B} = \begin{bmatrix} \mathbf{0} \\ \mathbf{M}^{-1}\mathbf{U} \end{bmatrix} \quad (6)$$

where  $\mathbf{C}$  and  $\mathbf{D}$  are formed appropriately so that linear combinations of the system states  $\mathbf{x}$  and inputs  $\mathbf{u}$  form the system outputs  $\mathbf{y}$ . The transfer function matrix  $\mathbf{H}$  can be formed from the system in Equation (5), at frequency  $\omega_i$ , as

$$\mathbf{H}(\omega_i) = \mathbf{C}(j\omega_i \mathbf{I} - \mathbf{A})^{-1} \mathbf{B} + \mathbf{D} \quad (7)$$

where  $j$  given by  $j^2 = -1$  is the imaginary number and  $\mathbf{I}$  the identity matrix of appropriate dimension.

In the calibration procedure equalised damping is imposed on the experimentally identified system  $\Sigma_X$ , defined as the quadruple  $\{\mathbf{A}_X, \mathbf{B}_X, \mathbf{C}_X, \mathbf{D}_X\}$ , and the FE system in order to avoid mode pairing, but also to obtain a smooth deviation metric [9]. To this end, the experimentally identified system  $\Sigma_X$  is transformed to diagonal form by a similarity transformation [29], e.g. the eigenvector matrix  $\mathbf{X}$  of the eigenvalue problem  $\mathbf{A}_X \mathbf{X} = \mathbf{X} \Lambda$  where  $\Lambda$  is the diagonal eigenvalue matrix. Then  $\mathbf{X}^{-1} \mathbf{A}_X \mathbf{X} = \tilde{\mathbf{A}}_X = \text{diag}(\lambda_i)$  where  $\lambda_i$  is the  $i$ :th complex valued system pole for  $i = 1, \dots, n$ . For small damping the relative damping is  $\xi_i = -\mathbb{R}(\lambda_i)/|\mathbb{C}(\lambda_i)|$  with  $|\cdot|$  representing the absolute value and  $\mathbb{R}(\cdot)$  and  $\mathbb{C}(\cdot)$  representing the real and complex part of an imaginary number, respectively. In the damping equalisation step, the modal damping is set to a fixed value for all modes, i.e.  $\xi_i = \xi_0 \forall i$ . A new state space system is then obtained, replacing  $\Sigma_X$ , with the quadruple set  $\Sigma = \{\tilde{\mathbf{A}}_X, \mathbf{X}^{-1} \mathbf{B}_X, \mathbf{C}_X \mathbf{X}, \mathbf{D}_X\}$  with  $\tilde{\mathbf{A}}_X = \text{diag}(\tilde{\lambda}_i)$  and

$$\tilde{\lambda}_i = \mathbb{C}(\lambda_i)(-\xi_0 + i) \quad \forall \mathbb{C}(\lambda_i) > 0, \quad \tilde{\lambda}_i = \mathbb{C}(\lambda_i)(\xi_0 + i) \quad \forall \mathbb{C}(\lambda_i) < 0. \quad (8)$$

For the FE model with given mass  $\mathbf{M}$  and stiffness  $\mathbf{K}$  matrices it is possible to impose the same level of relative damping by forming the modal viscous damping as described in [1]

$$\mathbf{V} = \mathbf{M} \mathbf{X} \text{diag}(m_i^{-1}) \text{diag}(2\xi_0 m_i \Omega_i) \text{diag}(m_i^{-1}) \mathbf{X}^T \mathbf{M}, \quad i = 1, \dots, m \quad (9)$$

where  $\Omega_i$  are the eigenfrequencies,  $m_i$  the modal masses and  $X$  the eigenvector matrix from the undamped eigenvalue problem of the system in Equation (4),  $\mathbf{K}X = \mathbf{M}X\text{diag}(\Omega_i^2)$ . It should be noted that in this paper equalised damping is only applied to the modes in the frequency range of interest  $\omega_i \in [\omega_{low}, \omega_{high}]$  for the experimental model.

Reduced order models must be formed from the full FE system as a practical consequence of the large size of industrial FE models. The calibration procedure works with physical parameters and thus parametrised mass and stiffness matrices are formed, which can be expressed as  $\mathbf{M} = \mathbf{M}(\mathbf{P})$  and  $\mathbf{K} = \mathbf{K}(\mathbf{P})$ , where the parameter vector  $\mathbf{P}$  is related to a normalised parameter vector  $\mathbf{p}$  and some fixed non-zero nominal parameter  $\mathbf{P}_0$  so that  $\mathbf{P} = \mathbf{P}_0(1 + \mathbf{p})$  holds [9]. The eigenvector matrix  $\mathbf{T}_0$  at the nominal parameter setting is used as a reduction basis and is kept constant during the calibration procedure, which is formed from the undamped eigenvalue problem of the system in Equation (4) such that residual modes, influencing the system in the frequency region of interest, are included [1]. The reduced mass and stiffness matrices at any parameter setting  $\mathbf{p}$  can then be formed as

$$\bar{\mathbf{M}}(\mathbf{p}) = \mathbf{T}_0^T \mathbf{M}(\mathbf{p}) \mathbf{T}_0, \quad \bar{\mathbf{K}}(\mathbf{p}) = \mathbf{T}_0^T \mathbf{K}(\mathbf{p}) \mathbf{T}_0 \quad (10)$$

with the reduced mass and stiffness matrices at the nominal parameter setting  $\mathbf{p}_0$  being represented by  $\mathbf{M}_0$  and  $\mathbf{K}_0$ . Gradients of the reduced mass and stiffness matrices can be formed as

$$\bar{\mathbf{M}}_{,j} = \mathbf{T}_0^T \left( \frac{d\mathbf{M}}{dp_j} \Big|_{p=p_0} \right) \mathbf{T}_0, \quad \bar{\mathbf{K}}_{,j} = \mathbf{T}_0^T \left( \frac{d\mathbf{K}}{dp_j} \Big|_{p=p_0} \right) \mathbf{T}_0 \quad (11)$$

for the  $j$ :th calibration parameter. From the first order expansions of the Taylor series of the reduced mass  $\bar{\mathbf{M}}$  and stiffness  $\bar{\mathbf{K}}$  matrices about  $\mathbf{p}_0$  it is possible to form a surrogate model that is linear in the parameters.

$$\tilde{\mathbf{M}}(\mathbf{p}) = \bar{\mathbf{M}}_0 + \sum_{j=1}^{n_p} (p_j - p_{j,0}) \bar{\mathbf{M}}_{,j}, \quad \tilde{\mathbf{K}}(\mathbf{p}) = \bar{\mathbf{K}}_0 + \sum_{j=1}^{n_p} (p_j - p_{j,0}) \bar{\mathbf{K}}_{,j} \quad (12)$$

Here  $p_{j,0}$  is the  $j$ :th parameter at the nominal setting. The FE transfer function representation  $\mathbf{H}_{FE}$ , which is used in the calibration procedure, can now be formed with use of Equation (7) from the state-space matrix quadruple  $\Sigma_{FE} = \{\tilde{\mathbf{A}}, \tilde{\mathbf{B}}, \tilde{\mathbf{C}}, \tilde{\mathbf{D}}\}$ , which is formed with a state transformation  $\mathbf{x} = \mathbf{T}\xi$  and with a viscous damping matrix  $\tilde{\mathbf{V}}$  formed as in Equation (9), such that

$$\tilde{\mathbf{A}} = \begin{bmatrix} \mathbf{0} & \mathbf{I} \\ -\tilde{\mathbf{M}}^{-1}\tilde{\mathbf{K}} & -\tilde{\mathbf{M}}^{-1}\tilde{\mathbf{V}} \end{bmatrix} \quad \tilde{\mathbf{B}} = \begin{bmatrix} \mathbf{0} \\ \tilde{\mathbf{M}}^{-1}\mathbf{T}^T \mathbf{U} \end{bmatrix} \quad \tilde{\mathbf{C}} = \begin{bmatrix} \mathbf{T} & \mathbf{0} \\ \mathbf{0} & \mathbf{T} \end{bmatrix} \quad \tilde{\mathbf{D}} = \mathbf{D}. \quad (13)$$

## 2.2 Model parameter uncertainties

From the deterministic calibration procedure a best parameter configuration  $\mathbf{p}^*$  is obtained, with respect to the identified model  $\Sigma$ . From a decision-making perspective it is important to assess the uncertainties in the obtained parameters such that confidence in the predictions can be obtained. In this paper bootstrapping [28] is used for stochastic model updating, proposed in [10, 11]. The procedure works by repeatedly drawing random datasets  $\mathbf{H}_X^b$  with replacement from the original data set  $\mathbf{H}_X$ , i.e.  $n_f$  random numbers  $\mathbf{d} = \{d_1, \dots, d_i, \dots, d_{n_f}\}$  are drawn from the uniform distribution on  $\mathbb{I} = \{1, 2, \dots, n_f\}$  and with the frequency lines  $\mathbb{F} = \{\omega_1, \dots, \omega_i, \dots, \omega_{n_f}\}$  in the experimental set  $\mathbf{H}_X$ ,  $\mathbf{H}_X^b$  can be formed such that

$$\mathbf{H}_X^b = \mathbf{H}_X(\omega_{d_i}) \quad \forall \mathbb{I}. \quad (14)$$

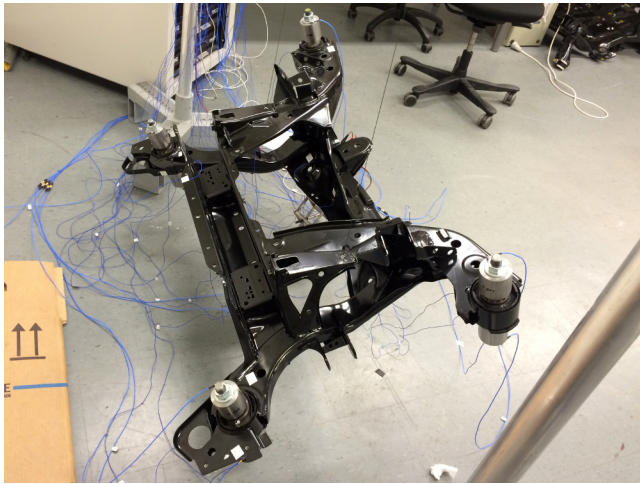
This procedure is repeated  $n_b$  times such that the deviation in Equation (3) is minimised  $n_b$  times for the different data sets. Thus  $n_b$  vectors of calibrated parameters  $\mathbf{p}_b$  will be obtained, from which the variance and expected value can be computed [10, 11].

## 3 Model preparation

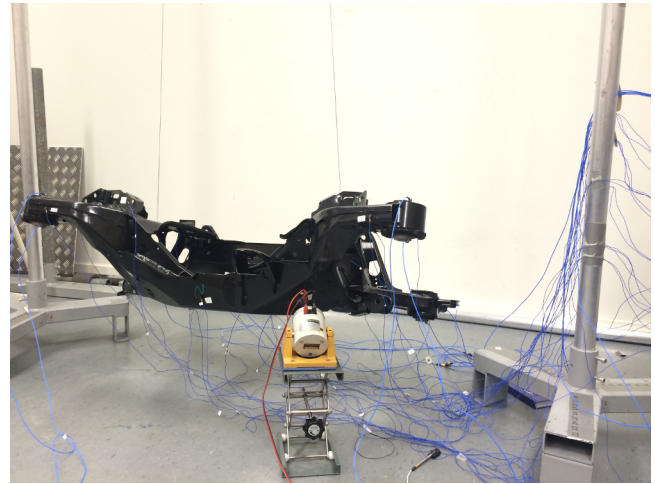
In this section the experimental modal analysis is explained along with the two FE models and the calibration parameter selection.

### 3.1 Experimental modal analysis

Vibration tests have been performed at Chalmers University of Technology Vibration Lab on three rear subframes of the Volvo XC90 with and without mass loading. Experiments, and results, on one subframe is reported here, but the procedures for the two other components were identical. The rear subframe with mass loading is visible in Fig. 3a and without mass loading in



(a) Configuration with mass loading with input at location 24



(b) Configuration without mass loading with input at location 24

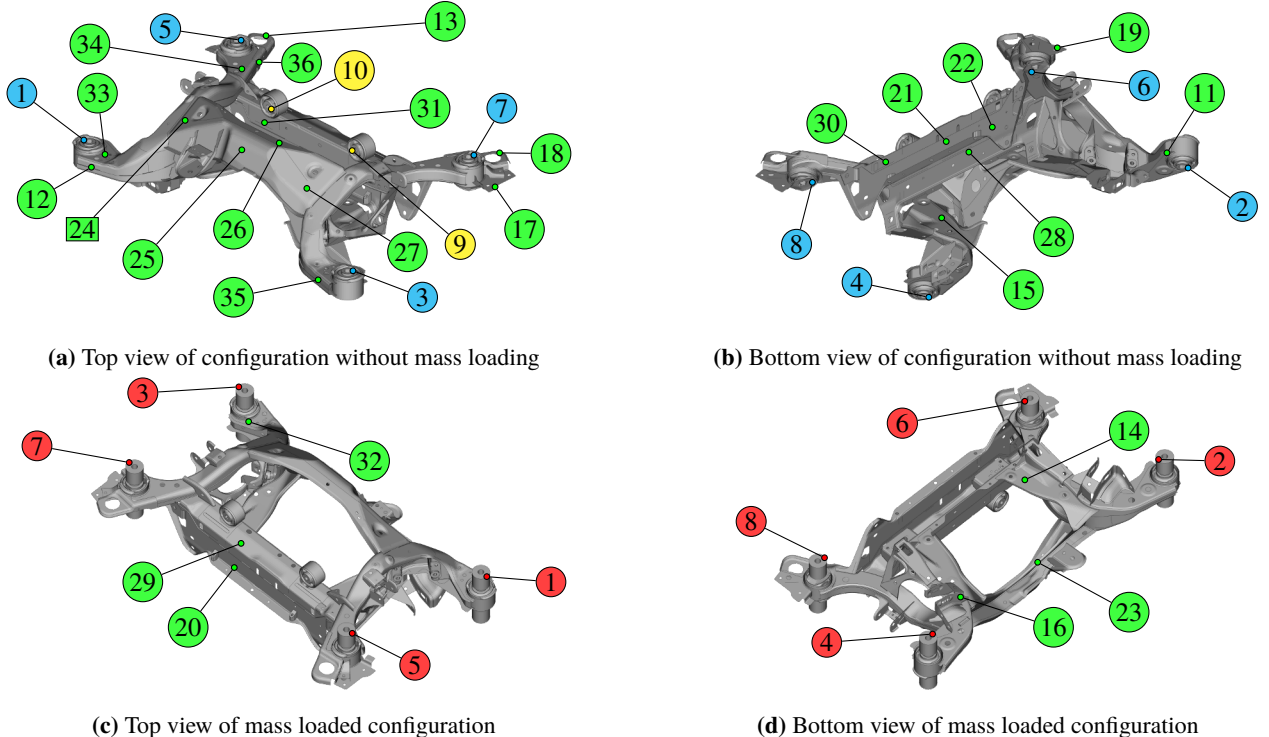
**Fig. 3** Rear subframe shown in (a) with mass loading, and in (b) without mass loading, both with input at location 24

Fig. 3b. The components were hung in long thin high-strength lines attached to steel springs on a supporting steel structure. Most of the quasi rigid body modes were kept under 2 Hz, while a support bouncing mode was kept under 5 Hz, i.e. the quasi rigid body modes were well under the first flexible mode of the component in both configurations.

An early version of the rear subframe FE model without modelled bushings was used in the pretest planning where 170 candidate locations were selected. Then 20 uniaxial sensor locations were found, out of the 170 candidate locations, with the set expansion EII [14, 15] method, for the 20 first flexible modes, with an added gramian rejection step for rejection of locations with similar information [16]. Six more uniaxial accelerometer positions were added for visualisation purposes. An additional 10 triaxial accelerometers were placed on the bushings, where 8 triaxial accelerometer locations were different for the two configurations. All sensor placements can be seen in Fig. 4. In Fig. 4a and 4b the configuration without mass loading is shown while the mass loaded boundary configuration is shown in Fig. 4c and 4d. Note that circular markings indicate accelerometers while a rectangle marking (only location 24) indicates input, with an additional direct accelerometer placed on the opposite side of the sheet metal. This was considered best practice as the metal plate was flat and thin (approximately 2 mm). The green colour coding indicate uniaxial accelerometers (accelerometers 11 to 36), while yellow, cyan and red indicate triaxial accelerometers (accelerometers 1 to 10). Accelerometers 9 to 36 were placed identically on both configurations while accelerometers 1 to 8 were placed directly on the bushings in the configuration without mass loading and thus had to be placed on the additional component attached to the bushings in the mass loaded configuration. In Fig. 4 cyan markings indicate positions for the configuration without mass loading while red indicate positions for the mass loaded configuration.

Two type of accelerometers were used, 10 triaxial PCB Piezotronic type 356A03 weighting 1 grammme each and 26 uniaxial PCB Piezotronic type PCB 352C22/NC weighting 0.5 grammes each. The uniaxial accelerometers were attached with synthetic wax while the triaxial accelerometers were glued. The orientation of the triaxial accelerometers around its own z-axis was approximated by sight, therefore data gathered from the x and y components of these accelerometers must be considered less accurate than the z component, which was normal to the structure. The accelerometer masses were included in the FE models. The shaker used in the vibration test was of Ling Dynamic Systems make and of type V201, with a metallic stinger approximately 5 mm in length, when attached, as recommended in [4]. The excitation force was measured with a Brüel&Kjær force sensor of type 8203 with an IEPE converter 2647B, attached to the component through a stinger attachment plate which was glued and had a mass of around 0.2 grammes. The force sensor and stinger attachment plate masses were not included in the FE models.

Two excitation methods were used for both configurations. Periodic chirp tests at various amplitudes were performed to assess the linearity of the systems to obtain proper excitation loads. In both configurations a frequency range from 20 to 800 Hz was used. The calibration data was collected with a stepped sine tests with multiple sinusoidal components excited simultaneously for reduced noise influence on the estimated parameters in the model updating procedure. For the mass loaded configuration a frequency region from 40 to 500 Hz was selected with 2000 frequency lines, due to the relatively high damping in the system. In the configuration without mass loading a frequency region from 60 to 500 Hz was selected with 3000 frequency lines, due to lower damping. In [9] the authors advise in selecting the frequencies based on the half-band width,  $\Delta\omega_i$ , of the eigenmodes. The half-band width for a damped structural resonance at a certain frequency  $\omega_i$  can be expressed as  $\Delta\omega_i = 2\xi_i\omega_i$  where  $\xi_i$  is the i:th relative modal damping. This is used in the calibration procedure, and initially in the EMA to find the

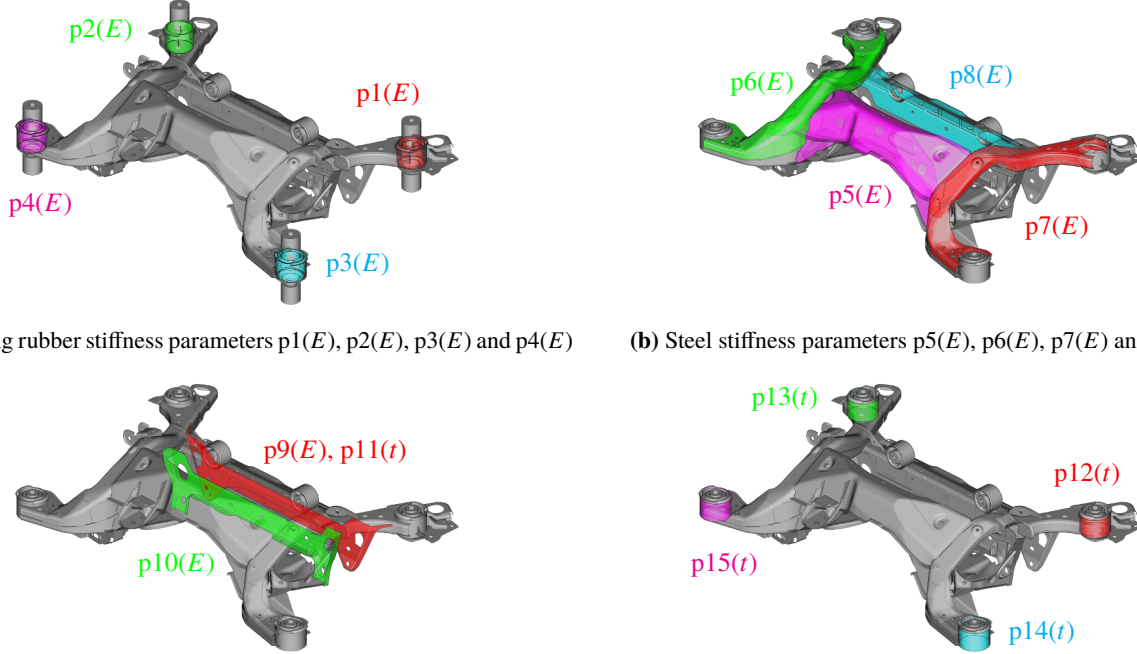


**Fig. 4** Top view of configuration without mass loading in (a) and bottom view in (b). Top view of mass loaded configuration in (b) and bottom view in (d). Circle markings indicate accelerometer locations and a rectangular marking indicate the input position. Input was normal to the surface, with a direct accelerance force and accelerometer sensor configuration. Green and yellow circles represent uniaxial and triaxial accelerometer locations, respectively, equal for both configuration cases. Cyan and red markings indicate triaxial sensors for the configuration without and with mass loading, respectively

number of frequency lines necessary. The EMA frequency lines were selected based on the improved frequency selection [17] method for system identification with N4SID [18].

The calibration procedure initially obtains a parameter configuration that minimises the deviation between the FE model and the experimentally identified system. It is therefore important to obtain a good mathematical model from the measured data. For the configuration without mass loading all accelerometers were used in the identification, from 60 to 350 Hz with 20 states. Low and high frequency residual modes were added to the obtained system and the system's  $\mathbf{B}$  and  $\mathbf{C}$  matrices re-estimated with additional data, from chirp measurements for the low frequency region from 20 to 60 Hz and stepped sine data for the high frequency region from 350 to 470 Hz. This produced a system that accurately predicted both resonance and antiresonance behaviour. For the mass loaded configuration only the bushing accelerometers, accelerometer 1 to 8 in Fig. 4c and 4d, were used initially for the system identification due to the many local bushing modes identified from the measurements, not visible in other channels. Thus an identified system with 40 states from 40 to 225 Hz was identified for 24 channels (8 first triaxial accelerometers). A low and high frequency residual system pole was added to the system and additional data from a chirp test from 20 to 40 Hz and stepped sine test from 225 to 250 Hz was used to re-estimate the system's  $\mathbf{B}$  and  $\mathbf{C}$  matrices. In addition all 36 accelerometers, or 56 channels, throughout the frequency region from 20 to 250 Hz were used in the re-estimation for a system with more system outputs.

The channels for which the system identification model gave the poorest fit were used as validation data as raw data is used in the validation procedure. In Fig. 4, with  $x$ ,  $y$ , and  $z$  components for the triaxial sensors, the calibration channels selected from the 56 available channels for the mass loaded configuration were  $\{1_x, 1_z, 2_x, 2_z, 3_x, 3_z, 4_x, 4_z, 5_x, 5_z, 6_x, 6_y, 6_z, 7_z, 8_x, 8_z, 9_x, 11, 12, 16, 17, 18, 20, 21, 22, 25, 26, 28, 29, 33, 34, 35, 36\}$ . For the configuration without mass loading the following set was selected  $\{1_x, 1_y, 1_z, 2_x, 2_y, 2_z, 3_x, 3_y, 3_z, 4_x, 4_y, 4_z, 5_y, 5_z, 6_y, 6_z, 8_z, 10_x, 11, 12, 13, 15, 16, 17, 18, 19, 20, 21, 22, 23, 25, 26, 27, 28, 29, 30, 31, 32, 33, 34, 35, 36\}$ . Approximately 60 % and 75 % of the channels were used for calibration in the configuration with and without mass loaded boundaries, respectively.



**(a)** Bushing rubber stiffness parameters  $p1(E)$ ,  $p2(E)$ ,  $p3(E)$  and  $p4(E)$       **(b)** Steel stiffness parameters  $p5(E)$ ,  $p6(E)$ ,  $p7(E)$  and  $p8(E)$

**(c)** Steel stiffness  $p9(E)$ ,  $p10(E)$  and thickness  $p11(t)$  parameters      **(d)** Steel thickness parameters  $p12(t)$ ,  $p13(t)$ ,  $p14(t)$  and  $p15(t)$

**Fig. 5** Parametrisation of the FE models with  $E$  representing stiffness and  $t$  thickness, in a) for the mass loaded configuration and in b), c) and d) for the configuration without mass loading. Parameters  $p1$  to  $p4$  were also parametrised in the configuration without mass loading

### 3.2 Finite element models

The rear subframe FE model, shown in Fig. 4 and 5, with and without mass loaded boundaries, consisted mainly of shell elements with the bushings modelled with an isotropic linear material model with solid elements, and consisted of over 600,000 degrees of freedom. The model was assumingly verified. The same FE model was used in the mass loaded boundary configuration where an additional heavy component was attached to the bushings. The additional component, shown in reality in Fig. 2c and as an FE model in the assembly in Fig. 2d, was designed to be simple to model with high accuracy. It is a simple cylinder with two different outer radii dimensions with a hole through its centre. It was made out of steel and each piece had a mass of 1 kg. Two such components were attached with bolts to each bushing of interest of the subframe, shown in Fig. 2d for one bushing, which had 6 bushings in total of which four were of interest in this study. MSC Nastran was used to establish the mass and stiffness matrices from the FE models.

### 3.3 Parameter selection

In the mass loaded boundary configuration only the rubber stiffness parameters were used in the calibration and all other model parameters were fixed to their nominal values. The parametrisation for the four bushings can be seen in Fig. 5a. For the configuration without mass loading 10 additional parameters were selected, in addition to the bushing parameters, which are shown in Fig. 5b to 5d. All other parameters, not highlighted, were fixed to their nominal values. The inverse Fisher information matrix (FIM) [30] was used in an identifiability analysis to fix parameters that would render the calibration problem unidentifiable. From this study it was found that parameter  $p12$  should be fixed. Two parameter types were used, material stiffness and shell element thickness. In the deterministic calibration most parameters were constrained to approximately 25 %, upper and lower bound, of their nominal setting, with some deviations.

It is known that rubber is a nearly incompressible material and therefore with a Poission's ratio approaching  $\nu = 0.5$ . With a value of  $\nu$  very close to 0.5, linear material FE models become overly stiff [31]. It was found that  $\nu$  was highly identifiable but did not give a smooth calibration metric and could thus not be used as a free parameter. A value of  $\nu = 0.49$ , as a best guess, was therefore fixed in all the model updating procedures.

**Table 1** Nominal parameters, denoted *Nom.*, along with three calibration results. Calibrated parameters for the mass loaded configuration denoted  $FE_{mass}$ , configuration without mass loading with calibration up to 265 Hz denoted  $FE_{265}$  and up to 350 Hz denoted  $FE_{350}$ . The mean value and coefficient of variation (%) of the bootstrapping procedure is denoted with superscript  $\mu$  and  $COV$ , respectively, i.e.  $FE_{mass}^\mu$  and  $FE_{mass}^{COV}$ . Empty fields (-) represent fixed parameters in that particular calibration. In this table  $E$  represent material stiffness and  $t$  denote thickness

#	Parameter	<i>Nom.</i>	$FE_{mass}$	$FE_{265}$	$FE_{350}$	$FE_{mass}^\mu$	$FE_{mass}^{COV}$	$FE_{265}^\mu$	$FE_{265}^{COV}$	$FE_{350}^\mu$	$FE_{350}^{COV}$
p1	$E$ [MPa]	5.00	4.01	4.01	4.62	3.67	0.72	-	-	4.98	0.39
p2	$E$	5.00	3.82	3.82	7.01	3.48	0.85	-	-	5.25	0.11
p3	$E$	5.00	2.83	2.83	5.83	2.69	0.94	-	-	-	-
p4	$E$	5.00	2.41	2.41	5.41	2.94	1.19	-	-	-	-
p5	$E$ [GPa]	210.00	210.00	192.32	192.32	-	-	196.44	0.99	-	-
p6	$E$	210.00	210.00	208.01	208.01	-	-	198.91	0.13	-	-
p7	$E$	210.00	210.00	240.73	240.73	-	-	228.60	0.09	-	-
p8	$E$	210.00	210.00	222.41	222.41	-	-	249.11	1.73	-	-
p9	$E$	210.00	210.00	250.82	250.82	-	-	264.38	3.86	-	-
p10	$E$	210.00	210.00	166.57	204.78	-	-	162.60	3.10	189.15	0.10
p11	$t$ [mm]	1.80	1.80	1.46	1.46	-	-	1.35	5.81	-	-
p12	$t$	1.40	1.20	1.40	1.40	-	-	-	-	-	-
p13	$t$	1.40	1.20	1.40	3.67	-	-	-	-	2.56	0.71
p14	$t$	1.40	1.20	1.40	1.81	-	-	-	-	1.75	1.12
p15	$t$	1.40	1.20	1.40	1.61	-	-	-	-	1.80	0.74

## 4 Calibration and validation results

The nominal and updated parameters from the deterministic calibration, and the mean value and coefficient of variation (COV, %) from the bootstrapping calibration are shown in Table 1 with the table order illustrating the calibration order, i.e. mass loaded configuration first followed by the configuration without mass loading up to 265 and 350 Hz in a second and final step, respectively. Thus, three calibrations were performed in total. Empty fields (-) denote fixed parameters in that particular calibration. In an initial step the mass loaded configuration was calibrated from 40 to 225 Hz so that the bushings' rubber stiffness could be estimated, i.e. parameters  $p1$  to  $p4$ . All other parameters were fixed to their nominal values, where parameters  $p12$  to  $p15$  were set to 1.20 mm. These four parameters were manually updated to a nominal setting of 1.40 in the calibration of the configuration without mass loading. The configuration without mass loading was first calibrated from 60 to 265 Hz, with updated bushing parameters, by updating parameters  $p5$  to  $p11$ . Updated parameters  $p5$  to  $p11$  were then used as nominal parameters in the final calibration from 60 to 350 Hz where parameters  $p1$ ,  $p2$ ,  $p10$ ,  $p13$ ,  $p14$  and  $p15$  were updated. Parameter  $p12$  was kept fixed in all three calibrations. Throughout the results section the deterministic calibration parameters  $p^*$  are used in the results, denoted after their respective model as in Table 2.

In Table 1 it can be seen that the mean value of the bootstrapping results, which are based on  $n_b = 20$  repeated calibrations, differ somewhat from the deterministic calibrated estimates. This is expected as the raw data is used in the bootstrapping calibration, which have significant noise levels around the low frequency anti-resonances for some channels, see Fig. 9b. Furthermore, the identified model used in the deterministic calibration does not perfectly fit test data in all channels, especially around the anti-resonances, and a difference is therefore to be expected. The parameters are stable, as indicated by the COV in Table 1, with parameters  $p9$ ,  $p10$  and  $p11$  for calibration  $FE_{265}$  slightly higher than than the others, approximately from 3 to 6 %. Running at least  $n_b = 100$  bootstrap calibrations is suggested in [28], which was not feasible due to the large datasets. It is likely that the variation would have decreased if  $n_b$  had been increased.

It can be seen in Table 1 that the two calibrated parameters  $p1$  and  $p2$  in the mass loaded configuration, visualised in Fig. 5a, are considerably stiffer than  $p3$  and  $p4$ . This is a consequence of making the FE model fit experimental data so that the modes shown in Fig. 7b to 7j would correspond to what was found experimentally. This is possibly a model inadequacy given that the bushings are different for these two set of parameters, i.e.  $p1$  and  $p2$  correspond to bushing 2 shown in Fig. 2b while  $p3$  and  $p4$  correspond to bushing 1 shown in Fig. 2a. Bushing 2 has an additional mass attached to it, and is less stiff in one direction. It is also possible that the bushing parameters to some extent acted as surrogate parameters due to other model parameters being fixed.

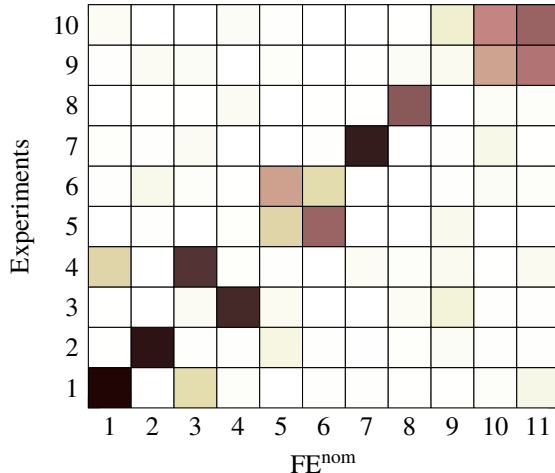
In Table 2 the eigenfrequencies of the first eleven flexible modes are shown for the configuration with and without mass loading, along with their masses. It can be seen that for the mass loaded configuration the nominal results are very different

**Table 2** First 11 flexible eigenfrequencies (Hz) for the two different configurations. Experimental eigenfrequencies for the configuration with and without mass loading denoted  $Exp_{mass}$  and  $Exp$ , respectively. Nominal FE models for the two configurations denoted with superscript *nom*.  $FE_{mass}$  denote mass loaded calibration.  $FE_{265}$  denote calibration up to 265 Hz and  $FE_{350}$  calibration up to 350 Hz for the configuration without mass loading.  $\Delta_{mass}$  (%) represent the relative difference between  $FE_{mass}$  and  $Exp_{mass}$ , and  $\Delta_{265}$  (%) and  $\Delta_{350}$  (%) the relative difference between  $Exp$  and  $FE_{265}$  and  $FE_{350}$ , respectively. Masses for the experimental set-ups and the different models is also shown

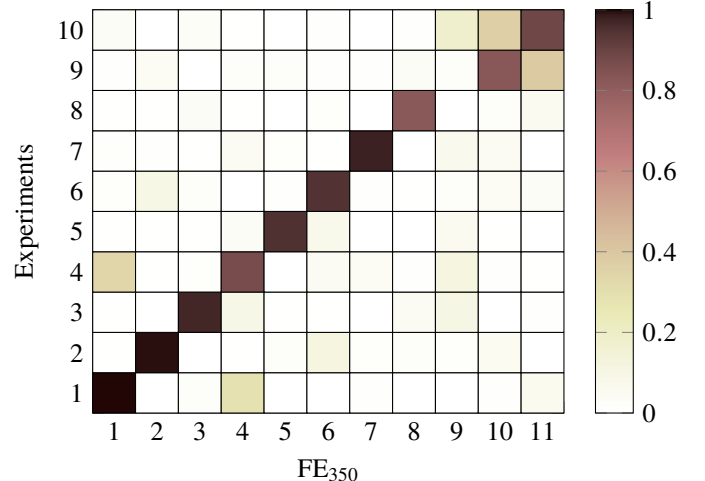
Mode	$Exp_{mass}$	$FE_{mass}^{nom}$	$FE_{mass}$	$\Delta_{mass}$ [%]	$Exp$	$FE^{nom}$	$FE_{265}$	$\Delta_{265}$ [%]	$FE_{350}$	$\Delta_{350}$ [%]
1	40.95	46.45	41.62	1.64	76.82	78.20	76.86	0.05	76.90	0.10
2	-	48.16	42.92	-	160.54	158.18	160.53	0.01	160.63	0.06
3	52.07	53.92	51.95	0.23	193.08	194.63	193.13	0.03	192.62	0.24
4	59.12	78.60	61.00	3.18	195.25	196.97	195.40	0.08	196.24	0.51
5	63.21	80.03	62.92	0.46	204.94	207.37	206.29	0.66	205.59	0.32
6	66.07	82.50	65.58	0.74	210.84	208.84	210.84	0.00	210.71	0.06
7	-	84.96	67.92	-	240.93	241.10	239.62	0.54	240.13	0.33
8	71.84	86.42	70.26	2.20	254.36	254.27	253.34	0.40	255.99	0.64
9	74.64	88.03	71.90	3.67	-	293.76	268.52	-	290.45	-
10	110.59	116.27	111.26	0.61	306.89	304.23	278.47	9.26	310.18	1.07
11	118.19	126.17	117.79	0.34	320.09	316.98	304.01	5.02	315.46	1.45
Mass	37.18	37.01	37.01		26.80	26.73	26.51		26.87	

from what is experimentally identified. It should be noted that mode 2 is very close to mode 1, in the experimental data, and could not be identified, i.e. that particular mode has mode multiplicity 2, show in Fig. 7b and 7c. The same holds for mode 6 and 7, shown in Fig. 7g and 7h. FE results indicate to that mode 4 and 5, and 8 and 9 are also paired, as seen from their modeshapes shown in Fig. 7. The calibrated  $FE_{mass}$  has a much better correspondence to experimental data compared to the nominal model  $FE_{mass}^{nom}$  which is also indicated by the deviation metric. The deviation metric between the experimental data  $Exp_{mass}$  and the nominal FE model  $FE_{mass}^{nom}$  is 0.90 and 1.02 for the calibration and validation, respectively. The updated model has a deviation metric of 0.44 and 0.50 for the calibration and validation, respectively. Thus an improvement of 51 % is seen in both the calibration and validation metrics. Note that a deviation of zero indicates perfect fit, but there is no upper bound. Therefore, even if there exist a model inadequacy the updated model makes good predictions and the bootstrapping results show a low variation in the parameters, as seen in Table 1, and hence the updated parameters are considered reliable.

From Table 2 it looks as if the nominal configuration without mass loading,  $FE^{nom}$ , correlates well with the experimental model, but from the modal assurance criterion (MAC) [32] analysis in Fig. 6a it can be seen that there is a mode switch between mode 3 and 4, and mode 5 and 6. Also, some modes show a very low correlation and the last two modes have a high cross-correlation. The updated model  $FE_{350}$ , for which the MAC analysis is shown in Fig. 6b, shows a much better MAC correlation, even for the modes above 300 Hz. It should be noted that there is a mode in the FE results, not identified in the experiments around 290 Hz. It is shown in Fig. 8j and it can be seen that it is a very local mode in one bushing. It is therefore not controllable from the input position, and due to its high damping it would be very hard to identify from the raw data. Further in Fig. 8 it can be seen that in the last two modes, over 300 Hz, the bushings are considerably active. In order to capture the behaviour of the two modes above 300 Hz the stiffness parameter in the rubber bushings had to be increased. Thus parameters  $p3$  and  $p4$  were manually increased by 2 MPa and  $p1$  and  $p2$  used as free parameters in the last calibration step,  $FE_{350}$ . An explanation for this behaviour is that rubber is frequency dependent, i.e. its stiffness increases with frequency [3]. In the mass loaded configuration the bushing parameters are estimated towards a lower frequency compared to the calibration without mass loading, and therefore to capture the behaviour above 300 Hz for the configuration without mass loading the stiffness must be increased. The intermediate calibration step,  $FE_{265}$  does not show a good correlation for modes above the 8:th flexible modes, as seen in Table 2, due to them not being included in the model updating. Because rubber elasticity is frequency dependent [3], not updating the rubber parameters but including the modes which activate the bushings in a frequency region not of interest would have caused the other parameters to act as surrogate parameters, compensating for the deviation above 300 Hz. The deviation metric for the intermediate model  $FE_{265}$  was improved with 60 % for the calibration from 0.91 to 0.38. The validation metric was improved with 23 % from 1.25 to 0.97. It should be noted that the nominal model from which  $FE_{265}$  was updated included the updated bushing parameters, and that this is reflected in the deviation metric. The deviation metric for the last model calibration  $FE_{350}$  was improved with 71 % for the calibration from 0.88 to 0.26, with nominal model  $FE_{265}$ , but manually



(a) MAC correlation between experiments and  $FE^{nom}$



(b) MAC correlation between experiments and  $FE_{350}$

**Fig. 6** MAC correlation between the experimentally identified system and the nominal FE model  $FE^{nom}$  in (a) and calibrated FE model  $FE_{350}$  in (b), respectively

updated parameter  $p3$  and  $p4$ . The validation metric was improved with 33 % from 1.20 to 0.81. The improvement in the validation metric is notably lower compared to the calibration metric. One possible reason is that poorly estimated channels were placed in the validation data set.

In Fig. 9a one of the better channels is shown for raw data, identified model, nominal FE model, calibrated FE model up to 265 Hz and 350 Hz. Fig. 9b depicts one of the poorer channel estimates.

## 5 Conclusions

This paper considers model updating and parameter uncertainty quantification of a rear subframe of a Volvo XC90 (2015), with parametrised bushings to gain physical insight in the structure at hand. A mass loaded boundary configuration was utilised to make more accurate estimates of the bushing's rubber stiffness such as they would be in a coupled configuration. A good estimate of the bushing parameters have been achieved from the mass loaded configuration. This parameter setting is thought to provide a more realistic representation of how the rear subframe will behave when coupled to the BIW, and should therefore be kept in the configuration without mass loading even though it has been shown that such an FE model produces poor results for frequencies above 300 Hz, where local bushing modes become active. The rubber stiffness must be increased if a good correlation for modes above 300 Hz for the configuration without mass loading is sought. Future work includes coupling the rear subframe to a BIW and assess the predictive capabilities of such an assembly from CAE. The frequency region of interest in such a study will be lower than 300 Hz, and therefore the mass loaded configuration should provide a better rubber parameter estimation.

It is likely that the bushings could have been modelled with bushing elements instead of solid elements, but because physical insight into the structure was sought a solid model was used, and the added degrees of freedom were negligible from a computational perspective. Further it would have been of interest to use Poisson's ratio as a free parameter in the model updating procedure. The model was found to be very sensitive to it, but as it gave a non-smooth calibration metric it had to be fixed.

Model updating towards the two other measured components will be performed in a future study. It will be of interest to verify how well the parametrisation can capture the component variability, and asses the parameter uncertainty towards other experimental data. It is also of interest to find the correct bushing parameters for the other components, and asses how much they will differ from the component presented in this study.

The calibration, validation and bootstrapping has been performed using the open source MATLAB program FEMcali, downloadable from Mathwork's webpage at [www.mathworks.com](http://www.mathworks.com).

## Acknowledgement

Volvo Car Corporation is gratefully acknowledged for providing the funding for this paper.

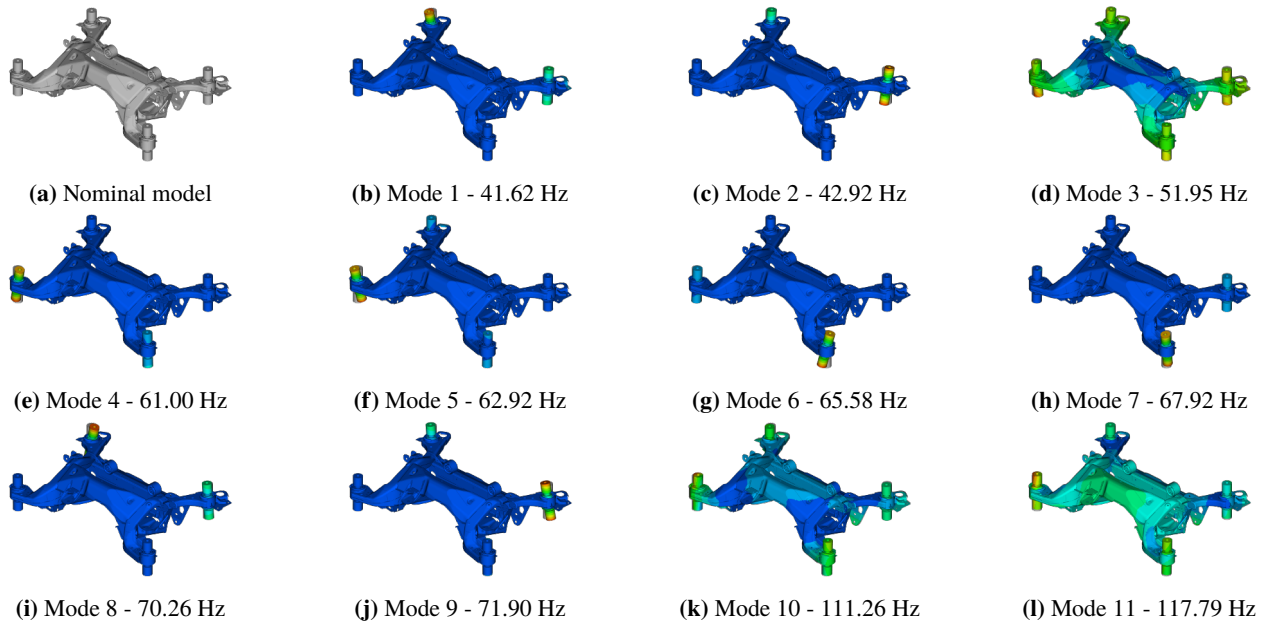


**Fig. 7** The mass loaded configuration (a), along with the 11 first calibrated flexible modes, from mode 1 (b) to mode 11 (l). Blue indicate small modal motion and red large motion

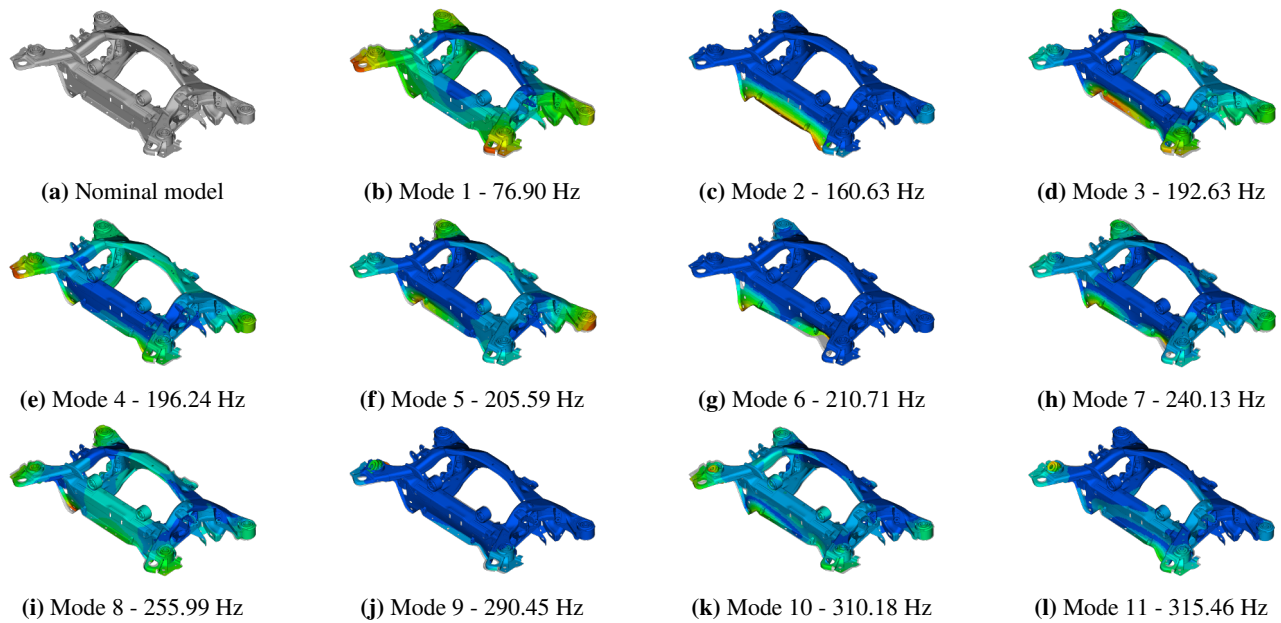
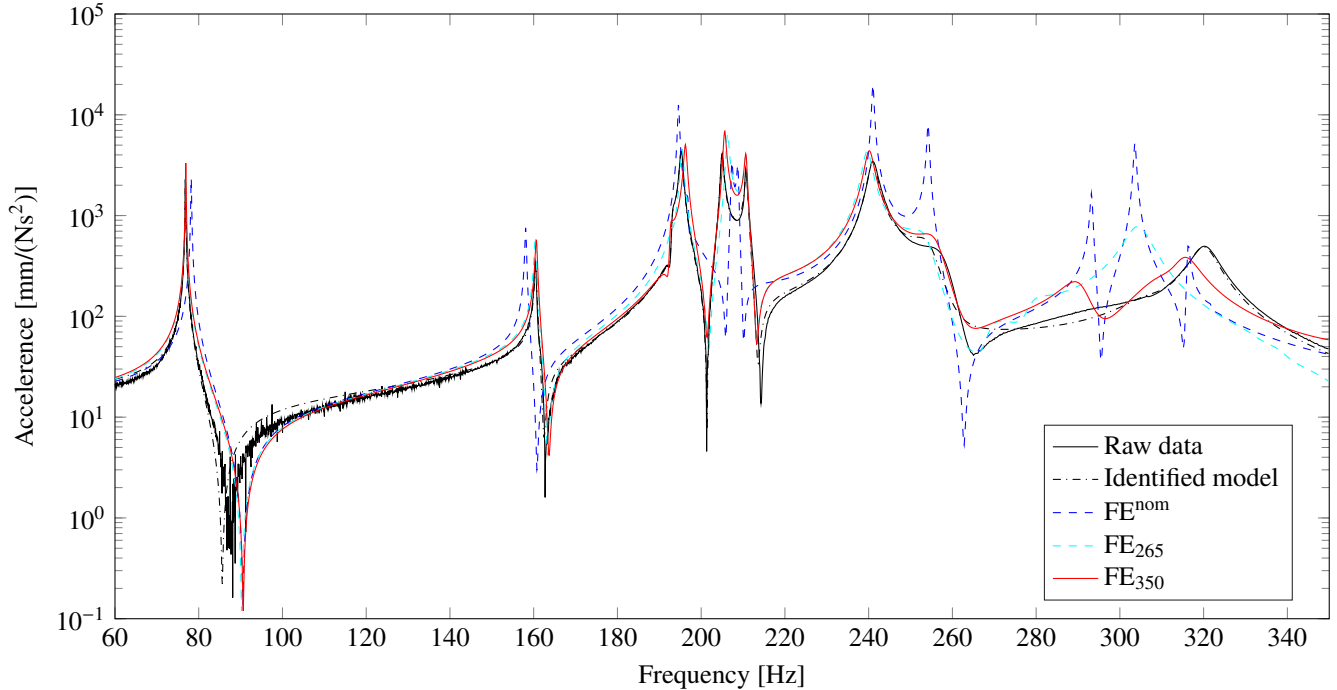
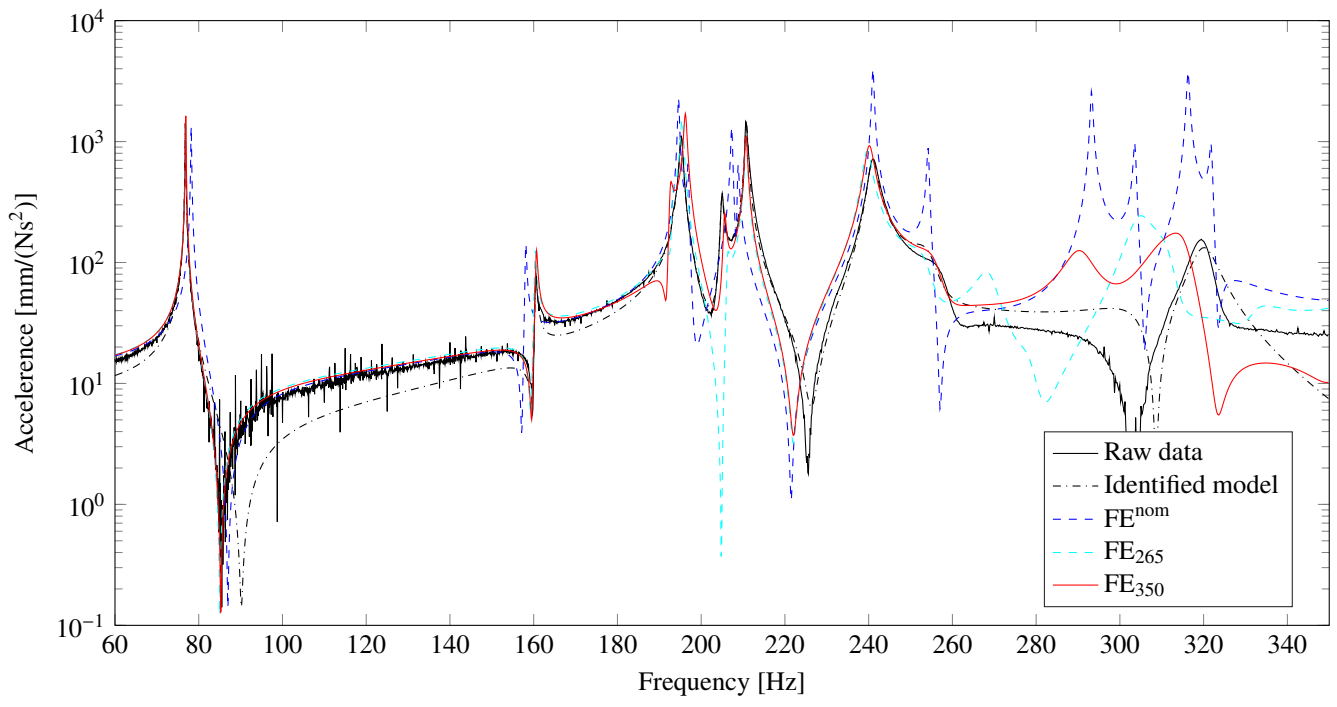


**Fig. 8** The configuration without mass loading (a), along with the 11 first calibrated flexible modes for model *FE<sub>350</sub>*, from mode 1 (b) to mode 11 (l). Blue indicate small modal motion and red large motion



(a) Input at position 24 and output at 4<sub>x</sub>



(b) Input at position 24 and output at 30

**Fig. 9** Frequency response functions of configuration without mass loading with raw data (black), identified model (dot dashed black),  $FE^{nom}$  (dashed blue),  $FE_{265}$  (dashed cyan) and  $FE_{350}$  (red). In (a) the input is at position 24 with output at position 4<sub>x</sub> and in (b) the input is at position 24 with output at position 30

## References

1. Roy R. Craig Jr. and Kurdila, A. J. *Fundamentals of Structural Dynamics*. 2nd Edition. Hoboken, N.J: Wiley, July 11, 2006. 744 pp.
2. Geradin, M. and Rixen, D. J. *Mechanical Vibrations: Theory and Application to Structural Dynamics*. 3rd Edition. Wiley, Feb. 16, 2015. 616 pp.
3. Jones, D. I. G. *Handbook of Viscoelastic Vibration Damping*. 1st Edition. Chichester ; New York: Wiley, July 6, 2001. 410 pp.
4. Ewins, D. J. *Modal Testing: Theory, Practice and Application*. 2nd Edition. Baldock, Hertfordshire, England; Philadelphia, PA: Wiley-Blackwell, Sept. 20, 2000. 576 pp.
5. Abrahamsson, T. J. S. et al. “Calibration and Validation of a Car Subframe Finite Element Model Using Frequency Responses”. In: *Topics in Modal Analysis, Volume 10*. Ed. by Mains, M. Conference Proceedings of the Society for Experimental Mechanics Series. Springer International Publishing, 2015, pp. 9–22.
6. Abrahamsson, T. et al. “Calibration and Cross-Validation of a Car Component Using Frequency Response Functions and a Damping Equalization Technique”. In: *26th International Conference on Noise and Vibration Engineering, ISMA 2014, Including the 5th International Conference on Uncertainty in Structural Dynamics, USD 2014*. 2014, pp. 2625–2640.
7. Gibanica, M., Abrahamsson, T. J. S., and Olsson, M. “Calibration, Validation and Uncertainty Quantification of Nominally Identical Car Subframes”. In: *Model Validation and Uncertainty Quantification, Volume 3*. Ed. by Atamturktur, S. et al. Conference Proceedings of the Society for Experimental Mechanics Series. Springer International Publishing, 2016, pp. 315–326.
8. Friswell, M. I. and Mottershead, J. E. *Finite Element Model Updating in Structural Dynamics*. Solid Mechanics and its Applications 38. Springer Netherlands, 1995.
9. Abrahamsson, T. J. S. and Kammer, D. C. “Finite Element Model Calibration Using Frequency Responses with Damping Equalization”. In: *Mechanical Systems and Signal Processing* 6263 (Oct. 2015), pp. 218–234.
10. Khorsand Vakilzadeh, M. “Stochastic Model Updating and Model Selection with Application to Structural Dynamics”. Doctoral Thesis. Chalmers University of Technology, 2016.
11. Yaghoubi, V. “System Identification of Large-Scale Linear and Nonlinear Structural Dynamic Models”. Doctoral Thesis. Chalmers University of Technology, 2016.
12. Larsson, K.-J. et al. “Calibration and Cross-Validation of a Car Component Model Using Repeated Testing”. In: *Model Validation and Uncertainty Quantification, Volume 3*. Ed. by Atamturktur, H. S. et al. Conference Proceedings of the Society for Experimental Mechanics Series. Springer International Publishing, 2015, pp. 339–350.
13. Echaniz Granado, I. “Model Calibration of a Vehicle Tailgate Using Frequency Response Functions”. Master’s Thesis. 2015.
14. Kammer, D. C. “Sensor Placement for on-Orbit Modal Identification and Correlation of Large Space Structures”. In: *Journal of Guidance, Control, and Dynamics* 14.2 (1991), pp. 251–259.
15. Kammer, D. C. “Sensor Set Expansion for Modal Vibration Testing”. In: *Mechanical Systems and Signal Processing* 19.4 (July 2005), pp. 700–713.
16. Gibanica, M., Abrahamsson, T. J. S., and Kammer, D. C. “Redundant Information Rejection in Sensor Localisation Using System Gramians”. In: *Topics in Modal Analysis & Testing, Volume 10*. Ed. by Mains, M. Conference Proceedings of the Society for Experimental Mechanics Series. Springer International Publishing, 2016, pp. 325–333.
17. Vakilzadeh, M. K. et al. “Experiment Design for Improved Frequency Domain Subspace System Identification of Continuous-Time Systems”. In: *IFAC-PapersOnLine*. 17th IFAC Symposium on System Identification SYSID 2015, Beijing, China, 19–21 October 2015 48.28 (2015), pp. 886–891.
18. McKelvey, T., Akcay, H., and Ljung, L. “Subspace-Based Multivariable System Identification from Frequency Response Data”. In: *IEEE Transactions on Automatic Control* 41.7 (July 1996), pp. 960–979.
19. Cunningham, J. R. and Ivey, D. G. “Dynamic Properties of Various Rubbers at High Frequencies”. In: *Journal of Applied Physics* 27.9 (Sept. 1, 1956), pp. 967–974.
20. Kennedy, M. C. and O’Hagan, A. “Bayesian Calibration of Computer Models”. In: *Journal of the Royal Statistical Society: Series B (Statistical Methodology)* 63.3 (Jan. 1, 2001), pp. 425–464.

21. Simoen, E., De Roeck, G., and Lombaert, G. "Dealing with Uncertainty in Model Updating for Damage Assessment: A Review". In: *Mechanical Systems and Signal Processing* 5657 (May 2015), pp. 123–149.
22. Ljung, L. *System Identification: Theory for the User*. 2nd edition. Upper Saddle River, NJ: Prentice Hall, Jan. 8, 1999. 672 pp.
23. Levenberg, K. "A Method for the Solution of Certain Non-Linear Problems in Least Squares". In: *Quarterly of Applied Mathematics* 2.2 (1944), pp. 164–168. JSTOR: 43633451.
24. Marquardt, D. W. "An Algorithm for Least-Squares Estimation of Nonlinear Parameters". In: *Journal of the Society for Industrial and Applied Mathematics* 11.2 (1963), pp. 431–441.
25. Andreasson, N., Evgrafov, A., and Patriksson, M. *An Introduction to Continuous Optimization*. Second edition. Lund, Sweden: Studentlitteratur AB, Dec. 23, 2013. 498 pp.
26. Mckay, M. D., Beckman, R. J., and Conover, W. J. "A Comparison of Three Methods for Selecting Values of Input Variables in the Analysis of Output from a Computer Code". In: *Technometrics* 42.1 (Feb. 1, 2000), pp. 55–61.
27. Yaghoubi, V. and Abrahamsson, T. "The Modal Observability Correlation as a Modal Correlation Metric". In: *Topics in Modal Analysis, Volume 7*. Ed. by Allemang, R. et al. Conference Proceedings of the Society for Experimental Mechanics Series. Springer New York, 2014, pp. 487–494.
28. Hastie, T., Tibshirani, R., and Friedman, J. *The Elements of Statistical Learning - Data Mining, Inference, and Prediction*. Springer Series in Statistics. Springer New York, 2009.
29. Golub, G. H. and Loan, C. F. V. *Matrix Computations*. Baltimore: The Johns Hopkins University Press, Dec. 27, 2012. 738 pp.
30. Kay, S. M. *Fundamentals of Statistical Signal Processing, Volume I: Estimation Theory*. 1st edition. Englewood Cliffs, N.J: Prentice Hall, Apr. 5, 1993. 625 pp.
31. Bathe, K. J. *Finite Element Procedures in Engineering Analysis*. Englewood Cliffs, N.J: Prentice Hall, Feb. 11, 1982. 736 pp.
32. Allemang, R. J. and Brown, D. L. "A Correlation Coefficient for Modal Vector Analysis". In: *Proceedings of the 1st IMAC*. International Modal Analysis Conference. 1982.